ACS OMEGA

http://pubs.acs.org/journal/acsodf

Article

Anion Exchange Composite Membranes Composed of Quaternary Ammonium-Functionalized Poly(2,6-dimethyl-1,4-phenylene oxide) and Silica for Fuel Cell Application

Vijayalekshmi Vijayakumar, Tae Yang Son, Kwang Seop Im, Ji Eon Chae, Hyoung Juhn Kim, Tae Hyun Kim, and Sang Yong Nam*

Cite This: *ACS Omega* 2021, 6, 10168−10179

Read Online

ACCESS | Metrics & More | Article Recommendations | Supporting Information

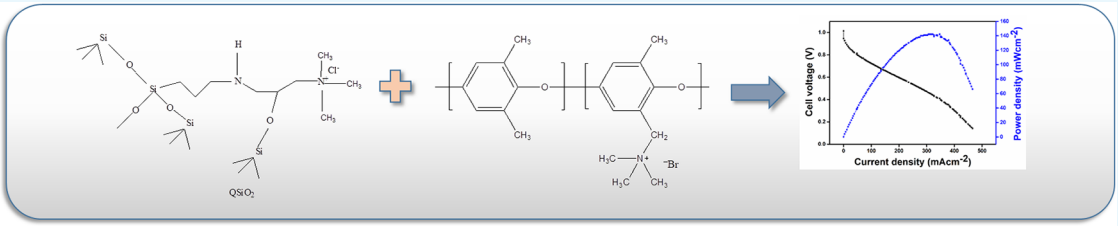

ABSTRACT: Anion exchange membranes (AEMs) with good alkaline stability and ion conductivity are fabricated by incorporating quaternary ammonium-modified silica into quaternary ammonium-functionalized poly(2,6-dimethyl-1,4-phenylene oxide) (QPPO). Quaternary ammonium with a long alkyl chain is chemically grafted to the silica *in situ* during synthesis. Glycidyltrimethylammoniumchloride functionalization on silica ($QSiO_2$) is characterized by Fourier transform infrared and transmission electron microscopic techniques. The QPPO/$QSiO_2$ membrane having an ion exchange capacity of 3.21 meq·g^{-1} exhibits the maximum hydration number (λ = 11.15) and highest hydroxide ion conductivity of 45.08 × 10^{-2} S cm^{-1} at 80 °C. In addition to the high ion conductivity, AEMs also exhibit good alkaline stability, and the conductivity retention of the QPPO/$QSiO_2$-3 membrane after 1200 h of exposure in 1 M potassium hydroxide at room temperature is about 91% ascribed to the steric hindrance offered by the grafted long glycidyl trimethylammonium chain in $QSiO_2$. The application of the QPPO/$QSiO_2$-3 membrane to an alkaline fuel cell can yield a peak power density of 142 mW cm^{-2} at a current density of 323 mA cm^{-2} and 0.44 V, which is higher than those of commercially available FAA-3-50 Fumatech AEM (OCV: 0.91 V; maximum power density: 114 mW cm^{-2} at current density: 266 mA cm^{-2} and 0.43 V). These membranes provide valuable insights on future directions for advanced AEM development for fuel cells.

1. INTRODUCTION

Growing attention has been paid globally in the development of a durable and highly efficient anion exchange polymer membrane in the area of fuel cells during the recent decade.[1−3] The faster electrokinetics, easier water management, fuel flexibility, reduced fuel cross-over, feasibility in the use of ample transition metal electrocatalysts (such as Co Ni, and Fe), and so forth make anion exchange membranes (AEMs) and anion exchange membrane fuel cells (AEMFCs) more attractive in last few years.[4−6] However, high hydroxide ion conductivity and good mechanical and chemical stability are the key challenges for the application of AEMs in AEMFCs.[7] Increasing the number of ion exchangeable sites and water molecules can impart high ion conductivity to the AEMs. On the other hand, excessive ion-exchange groups grafting in the polymers may damage the mechanical and thermal stability and result in inferior performance of the membranes.[8,9] Enhancement in the anion conductivity through increasing water uptake of the membranes can be enabled by incorporating hydrophilic inorganic fillers.[10]

Durability and stability are the most desirable properties of an AEM along with the physico and electrochemical properties.[11] Owing to the nucleophilicity and high basicity of cations, the polymer backbone is susceptible to the hydroxide ion attack, which leads to the undesirable loss of ion exchangeable sites and mechanical stability of the membranes. As a long-term challenge, much research effort has been focused on the aim of improving alkaline stability of cations in AEMs by fine-tuning the configuration of the cationic moieties on the polymer backbone.[12−14] Quaternary

Received: January 14, 2021
Accepted: March 22, 2021
Published: April 6, 2021

ACS Publications

© 2021 The Authors. Published by American Chemical Society

ammoniums are the normally used cations in AEMs and often suffer from the risk of degradation via direct nucleophilic substitution (SN2), E2 Hofmann elimination, ylide formation, and other rearrangement reactions under high pH conditions.[15]

The exploration of cationic group-grafted inorganic materials for AEMs has proved them as promising materials for various applications due to their well-proportioned properties such as high ionic conductivity, good mechanical properties, as well as enough durability owing to the synergistic effects of both the components. It has been noted that quaternized and imidazolium-functionalized POSS, quaternized mesoporous silica, and imidazolium-grafted titanate nanotube-based composite membranes displayed relatively higher ion exchange capacity (IEC), water absorption, conductivity, and thermal as well as mechanical properties.[2,16−19] Among the various inorganic materials, SiO_2 is extensively used due to its excellent chemical and physical (hydrophilic) properties. Wang et al. have proved that the use of 3-(trimethylammonium) propyl-functionalized silica resulted in high conductivity and thermal stability but its alkaline stability has not been publicized in their studies.[4] Tripathi et al. reported a hybrid composite AEM of a poly(vinyl alcohol) and 3-(2-aminoethylamino) propyl-trimethoxysilane-based silica precursor with adequate stabilities, water uptake and retention abilities, as well as flexibility. However, electrochemical and physicochemical properties are not yet to the level necessary for fuel cell applications.[20]

The grafting of long alkyl chains on to the surface of silica could ensure the membrane and polymer chain from being attacked by hydroxyl ions while increasing conductivity. The quaternary ammonium with alkyl aliphatic chain prompts nanophase separation and high performance.[21] Our previous work showed that the glycidyl trimethyl ammonium chloride has good alkaline stability and high ion conductivity.[22] In the present work, quaternary ammonium-functionalized silica ($QSiO_2$) was synthesized with glycidyl trimethylammonium chloride (GTMAC) (active electrophilic reagent), tetraethylorthosilicate (TEOS), and γ-aminopropyltriethoxysilane (γ-APTES) via electrophilic ring-opening reaction and was used as the hybrid material for the fabrication of polyphenylene oxide (PPO)-based nanocomposite AEMs. Silica was selected as the inorganic material due to its high surface area, water retention capacity, and high mechanical as well as thermal stability along with the ease of functionalization to tailor-made electrochemical requirements. The hydrophilic chains on the surface of $QSiO_2$ can aggregate at the polymer−filler interface with conductive groups on the polymer to form ionic clusters and facilitate ionic conduction in membranes. PPO is an excellent engineering plastic having outstanding stability against acids, bases, and other chemicals, low moisture absorption, excellent dimensional stability, and high mechanical strength.[20] The effect of the $QSiO_2$ content on the membrane properties such as thermal and mechanical stability, IEC, hydrolytic stability, conductivity, as well as alkaline stability was systematically investigated. The use of long alkyl chain-grafted silica in quaternized PPO maintained a high ionic conductivity and strong mechanical properties as well as chemical stability to the membranes. When applied in a H_2/O_2 single cell, the optimized AEM exhibits a maximum power density of 142 mW cm^{-2} at a current density of 323 mA cm^{-2} and 0.44 V.

2. RESULTS AND DISCUSSION

2.1. Structure and Morphology of $QSiO_2$. The Fourier transform infrared (FTIR) spectra of SiO_2 and $QSiO_2$ are shown in Figure 1. The characterized spectrum of SiO_2 shows

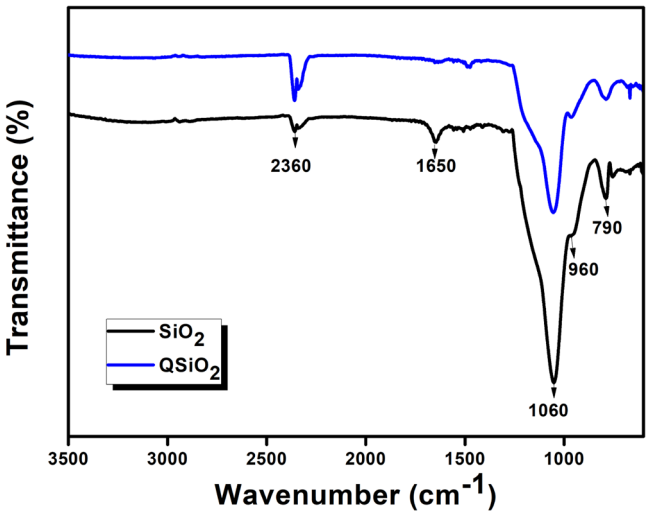

Figure 1. FTIR spectra of SiO_2 and $QSiO_2$.

a strong absorption band at 1060 cm^{-1} corresponding to Si−O−Si asymmetrical stretching and Si−O−Si symmetrical stretching at 790 cm^{-1}.[23,24] The shoulder appeared at 960 cm^{-1} in SiO_2 represents the Si−OH stretching while the peaks at 2360 and 1650 cm^{-1} are attributed to the C−H vibration and N−H stretching associated with aminopropyl triethoxy silane.[25] The doublet at 2360 cm^{-1} might also represent the traces of carbon dioxide absorbed by the quaternized amine present in the material. The increase in the intensity at 2360 cm^{-1} owing to the presence of the methyl group from GTMAC confirms the successful functionalization of SiO_2.

The high-resolution transmission electron microscopic (HRTEM) images of SiO_2 and $QSiO_2$ (Figure 2) show that the particles synthesized exhibit a size of 5−15 nm. The selected area electron diffraction (SAED) pattern of silica particles (Figure 2a′) shows the clear rings consisting of discrete spots, confirming their polycrystalline structure, whereas the structure transforms into an amorphous form (Figure 2b′) after modification with GTMAC. The C, N, and Cl elements appeared in the energy dispersive X-ray analysis (EDAX) spectra of $QSiO_2$ and their uniform distribution is observed in the compositional mapping images (Figure S1), further confirming successful quaternization of silica with GTMAC. These elements develop the trajectory path for ion conduction of the membranes.

2.2. Characterization of QPPO/$QSiO_2$ Composite Membranes. *2.2.1. Structural Analysis.* The chemical structure of quaternary ammonium-functionalized anion exchange hybrid membranes is confirmed by FTIR spectroscopy. Figure 3 shows the FTIR structure (normalized with respect to the C=C stretching of the phenyl group) of QPPO/$QSiO_2$-*X* membranes. In the FTIR spectra of QPPO, the broad absorption band centered at around 3500 cm^{-1} mainly results from the −NH stretching of quaternary ammonium groups as well as −OH stretching vibration possibly from bound water owing to the strong hydrophilicity of quaternary ammonium groups while the absorption bands

https://doi.org/10.1021/acsomega.1c00247
ACS Omega 2021, 6, 10168−10179

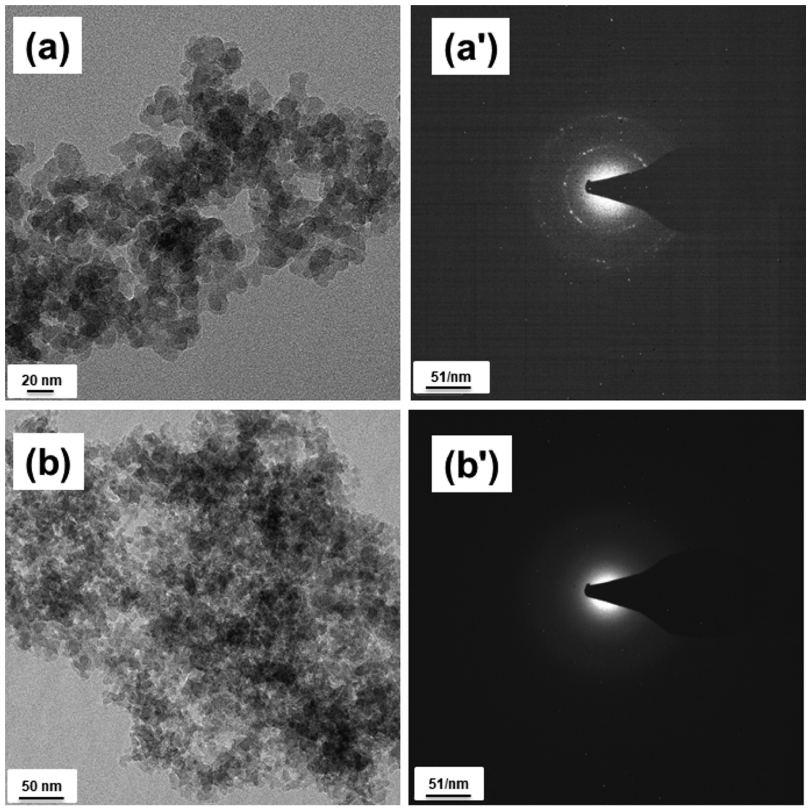

Figure 2. HRTEM images of (a) SiO_2 and (b) $QSiO_2$ and SAED patterns of (a′) SiO_2 and (b′) $QSiO_2$.

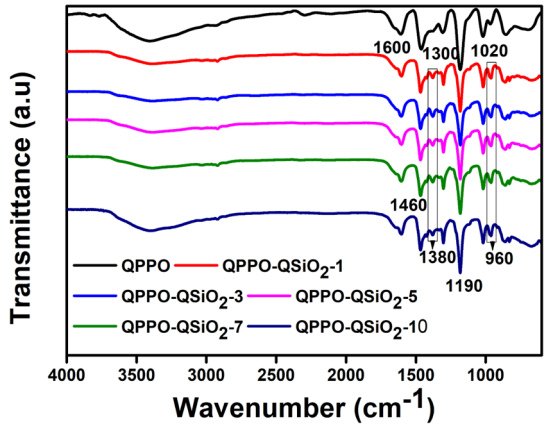

Figure 3. FTIR spectra of QPPO/$QSiO_2$-*X* composite membranes.

located at 1020, 1190, and 1460 cm^{-1} are ascribed to C−O and C−O−C stretching, as well as $-CH_2$ bending vibrations, respectively. The characteristic C═C stretching of the phenyl group and C−N stretching in the quaternization of PPO are observed at 1600 and 1300 cm^{-1} respectively.[22] The new absorption bands noticed at 1380 and 960 cm^{-1} in all the composite membranes excepting the pristine QPPO membrane corresponding to the N−H and Si−OH stretching associated with $QSiO_2$ confirm the successful formation of hybrid composite membranes.

2.2.2. Morphology. The microscopic cross-sectional morphology of the pristine QPPO and QPPO/$QSiO_2$-*X* membranes (*X* = 1, 3, 5, 7, 10 wt %) is shown in Figure 4. The cross-sectional image of the pristine QPPO membrane presents a relatively smooth surface without any pinholes or cracks. After the incorporation of $QSiO_2$, the membrane becomes rigid and dense in structure, as well as the aggregation becomes more evident at 10 wt % filler concentration. The presence of quaternary ammonium belonging to both QPPO and $QSiO_2$ contributes to the van der Waals force of interaction and hence the homogeneous distribution of $QSiO_2$ that may facilitate the formation of ion conductive channels. At high filler concentration, aggregation might block the ionic pathways. The elemental dot mapping also supported the high density of silica at higher filler loading (Figure S2). The results of EDAX analysis confirm the presence of Si and Cl only in QPPO/$QSiO_2$ composites.

The pristine QPPO, QPPO/$QSiO_2$-3, and QPPO/$QSiO_2$-7 membranes were morphologically analyzed using small angle X-ray scattering (SAXS) (Figure 4g). Two distinct scattering peaks were observed at 0.53 and 0.73 nm^{-1} in QPPO, suggesting the presence of ionic clusters, and the average inter ionic cluster distance obtained based on Bragg's law ($d = 2\pi/q_{max}$, where d is the Bragg spacing and q_{max} is the maximum scattering vector) varied from 8 to 12 nm. These scattering peaks or ionomer peaks are associated with well-defined microstructures due to the phase-separated morphology among hydrophilic and hydrophobic domains.[26] The appearance of two peaks may indicate short- and long-range ordered ionic clusters in the membrane structure. A similar structure is also reported by Becerra-Arciniegas et al., which is not fully understood.[27] In the presence of 3 wt % filler, no such scattering peaks were noticed, indicating that the filler reduces the intramolecular interactions among polymer chains and makes intermolecular interactions among the polymer and the filler. These interactions can cause the formation of an ionic cluster, thereby conducting channels inside the composite membrane. A small shoulder appeared in between 0.16 and 0.30 nm^{-1} in QPPO/$QSiO_2$-3 corresponding to the inter ionic

https://doi.org/10.1021/acsomega.1c00247
ACS Omega 2021, 6, 10168−10179

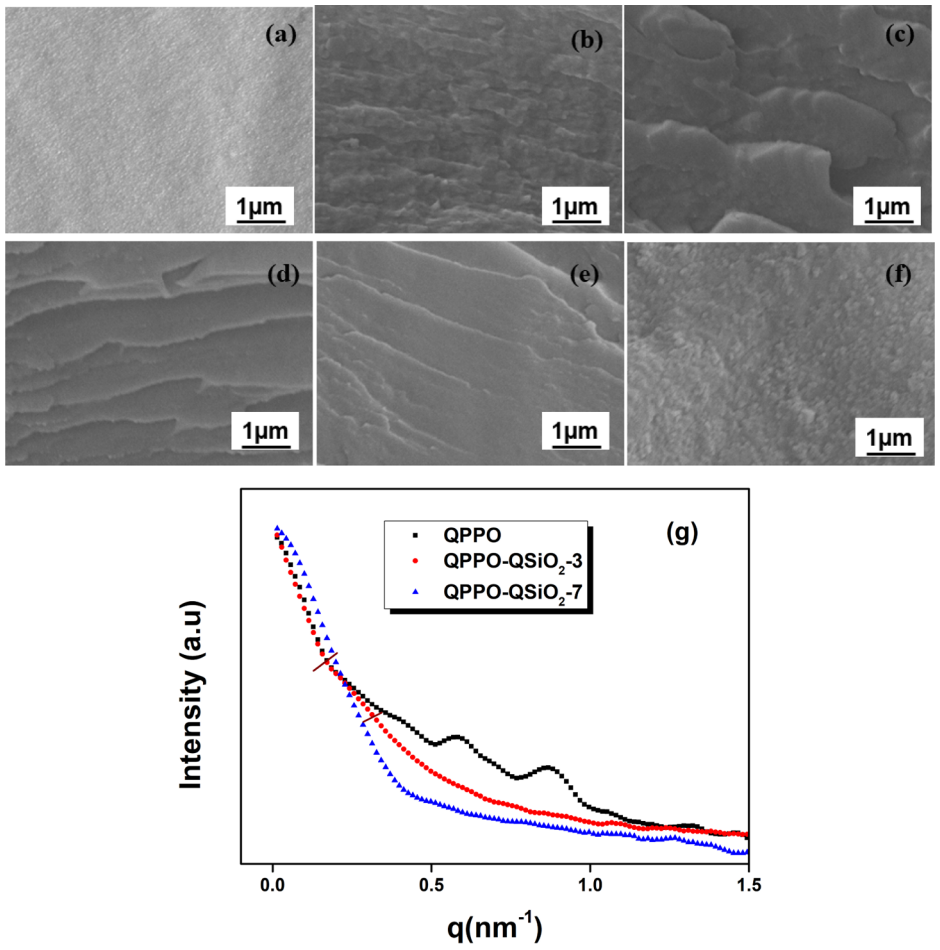

Figure 4. FESEM images of (a) QPPO, (b) QPPO/$QSiO_2$-1, (c) QPPO/$QSiO_2$-3, (d) QPPO/$QSiO_2$-5, (e) QPPO/$QSiO_2$-7, and (f) QPPO/$QSiO_2$-10 composite membranes and (g) SAXS profiles of QPPO-based dry composite membranes.

cluster spacing of about 30 nm, and it disappeared at higher concentration (7 wt %), which shows the presence of well-dispersed ionic clusters in the composite membranes. The absence of the scattering peak also suggests the presence of much smaller ionic clusters in the membrane. This result agrees with the AEMs reported elsewhere.[28−30] The presence of ionic cluster formation would have a strong impact on the ion transport properties in the anion exchange composite membrane, which will be investigated in the forthcoming section.

2.2.3. Thermal and Mechanical Properties. Good thermal stability of alkaline membranes is indispensable for the use of fuel cells. In Figure 5, the thermogravimetric analysis (TGA) thermograms of all the composite membranes show mainly three thermal decomposition regions under the nitrogen atmosphere. The first region below 200 °C with a weight loss of about 12−18% is ascribed to the loss of the residual solvent and absorbed water present in the membranes.[31] The second region from 200 to 280 °C revealed the cleavage of quaternary ammonium groups that occurred in the membranes. The result is comparable with other quaternary ammonium-modified membranes that indicate good thermal stability of the present membranes.[32,33] The final weight loss above 280 °C is related to the degradation of the polymer main chain.[22] Generally, the thermal stability increases when silica is incorporated in the organic polymer matrix. However, compared to QPPO, the composite membranes exhibit more

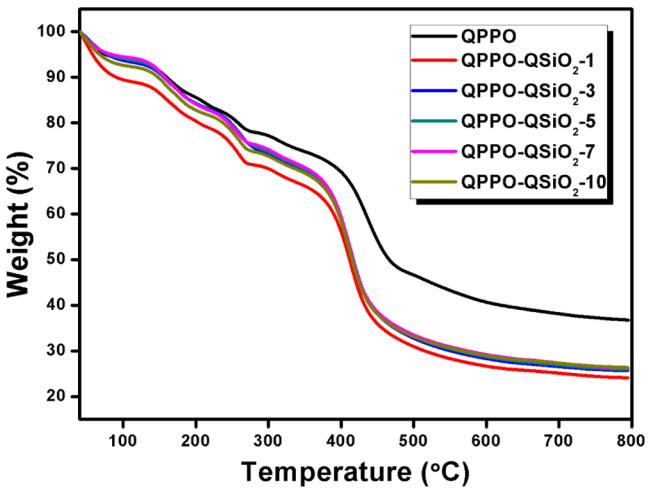

Figure 5. TGA thermograms of QPPO/$QSiO_2$ composite membranes.

weight loss due to the degradation of organic functional groups present on the surface of silica, which also promotes the degradation of the polymer matrix around the particles.[34] However, a slight increase in residue weight percentage and the temperature at which up to 60% weight loss occurred observed with an increase in filler content from 1 to 3 wt %. In the QPPO/$QSiO_2$-1 membrane, 60% weight loss is noticed at

https://doi.org/10.1021/acsomega.1c00247
ACS Omega 2021, 6, 10168−10179

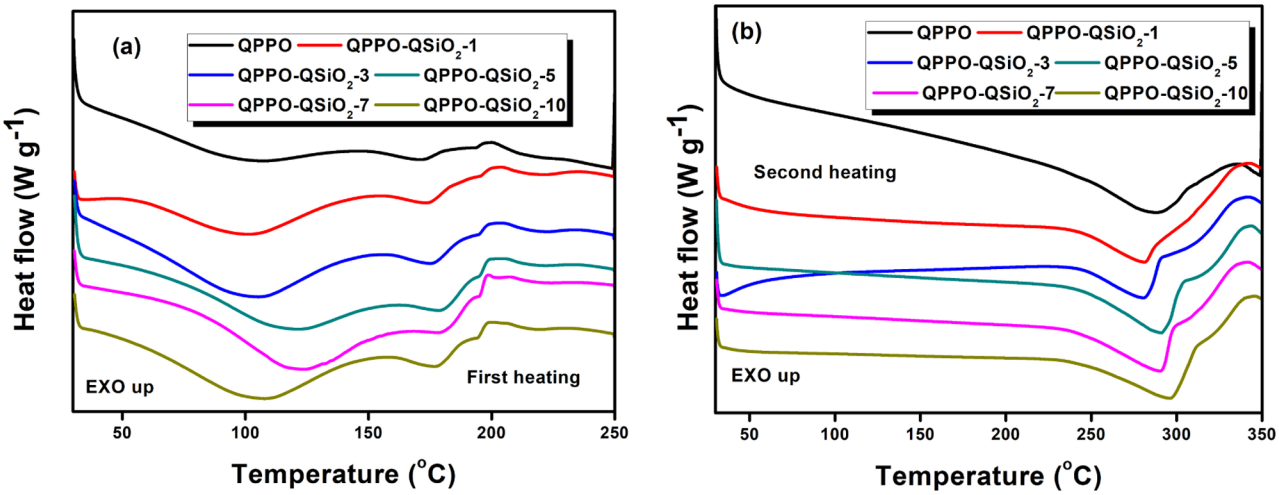

Figure 6. DSC (a) first and (b) second heating curves of QPPO/$QSiO_2$ composite membranes.

about 362 °C and the corresponding value of QPPO/$QSiO_2$-3 is 383 °C. This specifies that the addition of $QSiO_2$ can enhance the rigidity of the membranes to prevent them from degradation and increase their thermal stability. The same degradation characteristics has also been reported in the composite membranes based on polysulfone and quaternized polyhedral oligomeric silsesquioxane (QAPOSS).[17] 3 wt % loading is the optimal dosage, above that $QSiO_2$ has no significant effect on membranes' thermal stability which may be due to their compact (dense or closely packed) structure. In conclusion, all the membranes show enough thermal stability below 200 °C far beyond the range of AEMFC applications.

Figure 6a,b shows the first and second heating differential scanning calorimetry (DSC) curves of QPPO and QPPO/$QSiO_2$ composite membranes. All the membranes exhibit an endothermic event at around 100 °C and another at around 170−180 °C due to the evaporation of water and weakly bound solvent molecules, respectively. A small transition owing to the loss of the quaternary ammonium group has also been noticed at around 195 °C. The endothermic melting peaks in the region of 281−298 °C are observed in the second heating curve. In the case of composites, the peak position is shifted to the lower temperature, and the peak area is directly proportional to the crystallinity of the composites. The pristine QPPO shows a broad peak which then decreased upon the addition of the filler, revealing the reduction in crystallinity up to a concentration of 3%. This may be because of the physical and molecular changes formed by the nanofiller−polymer interaction which recommend the more stable membranes.

Table 1 presents the tensile strength and percentage elongation at break of the pristine QPPO and its composite membranes. The composite membranes display remarkable improvements in mechanical strength, exhibiting tensile strength values ranging from 25.4 to 42.1 MPa for QPPO/$QSiO_2$ membranes which are higher than those of neat QPPO (9.3 MPa) owing to the presence of a Si−O−Si inorganic network in the hybrid membranes. Furthermore, the composite membranes display lower elongation in comparison with the pristine membrane, showing that an increase in the filler leads to the restricted movement of polymer chains, probably due to the hydrophilic interactions among the quaternary groups of the polymer and filler. The enhanced mechanical strength indicates that quaternized silica particles are well-dispersed within the matrix below 3 wt % without significant aggregation. Further addition of a $QSiO_2$ nanofiller leads to the drop in mechanical strength as the compact/closely packed structure of filler dispersion adversely affects the polymer—filler wetting and interaction and the material becomes brittle. All the membranes show acceptable mechanical properties for fuel cell applications as per the membranes reported earlier.[35,36]

Table 1. Mechanical Property and IEC of the Composite Membranes

sample designation	tensile strength (RT, MPa)	elongation at break (RT, %)	IEC at 25 °C ($meq{\cdot}g^{-1}$)
QPPO	9.3 ± 0.5	25.3 ± 1.2	2.33 ± 0.03
QPPO/$QSiO_2$-1	35.1 ± 2.1	25.8 ± 3.2	2.56 ± 0.02
QPPO/$QSiO_2$-3	42.1 ± 0.8	22.7 ± 1.1	2.80 ± 0.03
QPPO/$QSiO_2$-5	31.3 ± 2.8	15.2 ± 2.0	3.05 ± 0.04
QPPO/$QSiO_2$-7	29.0 ± 1.4	13.1 ± 1.8	3.21 ± 0.02
QPPO/$QSiO_2$-10	25.4 ± 3.6	9.25 ± 1.7	3.13 ± 0.03

2.2.4. Water Uptake Behavior and IEC. Sufficient water content in AEMs facilitates the development of a percolating hydrated ionic phase domain for effective ion transport but the content should be controlled at a balanced level to eliminate undesired swelling and deterioration of mechanical properties. The water uptake and longitudinal swelling properties of the developed membranes are presented in Figure S3a,b. All the composite membranes show higher water absorption capacity than the pure QPPO membrane. The results indicate that the surface functionality of silica significantly facilitates the interaction with water molecules in the composite membranes. The change in swelling percentage is also consistent with the water absorption of the membranes. The swelling property is a critical factor to be considered for the performance of alkaline fuel cells because the mechanical property, ion migration, and dimensional stability depend greatly on it.[37] Both water uptake and swelling values are comparatively higher at 80 °C than at room temperature credited to the hygroscopic property and water retention associated with the quaternary ammonium group present in both QPPO and $QSiO_2$.[19] Moreover, the polymer chain mobility and free volume also contribute to the absorption of water into the membranes. A measurable reduction in water uptake and swelling noticed when the $QSiO_2$ content is above 7 wt % due to the over dosage of the

https://doi.org/10.1021/acsomega.1c00247
ACS Omega 2021, 6, 10168−10179

filler which inhibits chain mobility. The swelling percentage is relatively low [7−11% at room temperature (RT) and 11−22% at 80 °C], and taking the observation into account, membranes in this work are shown to be potentially attractive candidates in AEMs.[38−40]

In order to define the water absorption of the membranes accurately, the number of absorbed water molecules per ionic group (quaternary ammonium) (λ) are also calculated, and the values are presented in Table 2. A positive correlation among λ and hydroxide ion conductivity can be seen which demonstrates the main role of the hydration mechanism on anion conductivity. The more number of quaternary ammonium groups and high degree of hydrophilicity are favorable for high hydration number (λ) at a $QSiO_2$ concentration of 7 wt %. Performance of an ion exchange membrane in electrochemical devices is very much dependent on the nature of water, which is classified into free and bound water present. Free water has a weak interaction with the polymer chains and acts like bulk water. In turn, bound water is strongly bound to the polar moieties present in the polymer chain and additives such as quaternary ammonium and hydroxyl groups.[41] The hopping mechanism of conduction is mainly facilitated by bound water, whereas the diffusion or vehicular mechanism is facilitated by free water.[37] TGA analysis and water uptake results are used to find the state of water in the developed composite AEMs. The results obtained are given in Figure S4 and Table 2. As shown in Table 2, both bound and free water increase with the increase in filler content up to 7 wt % and then show a drop. The strong interaction among the quaternary ammonium groups and the water molecules aids enough binding sites to constrain water in the membrane which brings about high bound water content in QPPO/$QSiO_2$-7. At 10 wt % $QSiO_2$; due to the dense structure and asymmetric distribution, a reduction in water absorption and retention is noticed.

Table 2. Number of Water Molecules per Ionic Sites, Bound and Bulk Water and Activation Energy of the Composite Membranes

	number of water molecules per ionic site (λ)				
sample designation	RT	80 °C	bound water (%)	bulk/free water (%)	activation energy, E_a (kJ mol^{-1})
QPPO	4.15	8.77	1.68	15.72	9.15
QPPO/$QSiO_2$-1	6.47	9.72	1.82	27.98	9.45
QPPO/$QSiO_2$-3	7.22	10.69	1.92	34.48	10.59
QPPO/$QSiO_2$-5	8.12	10.82	1.95	42.65	16.06
QPPO/$QSiO_2$-7	9.09	11.15	2.15	50.35	16.46
QPPO/$QSiO_2$-10	8.59	10.74	2.03	46.37	17.08

Table 1 illustrates the IEC values of QPPO and its composite AEMs in the hydroxide form. It reveals about the nature of ionic charge responsible for the exchange of OH^- in terms of functional group equivalents present per unit dry weight of the membrane.[42] Therefore, IEC is an indirect measure of ion conductivity. It can be seen that the IEC values of composite membranes are in the range of 2.56−3.21 mmol g^{-1} and are higher than that of the pristine QPPO membrane (2.33 mmol g^{-1}). Increase in IEC values with the filler content is attributed to the availability of more ionic sites (quaternary ammonium) present in the membrane.[17] The reduction in the availability of the number of polar groups and free volume at a higher concentration (10 wt %) due to particle aggregation results in the reduction of IEC as well as water uptake.

2.2.5. Hydroxide Ion Conductivity and Alkaline Stability. Compared to the pristine QPPO membrane, the composite membranes show much higher conductivity (Figure 7a) due to the combined effects of enhanced IEC and water content which resulted from the introduction of $QSiO_2$. The hydrophilic conductive groups on the filler may possess strong attraction to the hydrophilic quaternary ammonium groups on PPO chains and strong repulsion to its hydrophobic backbones, which bring "seeds" guiding the microphase aggregation process at the polymer−filler interface and consecutively generate distinct paths to facilitate ion transport.[16] Moreover, the positive temperature—conductivity dependency exhibited by all the membranes as a result of quick migration of ionic clusters and high water and ion diffusivity suggests the thermally actuated conduction process in between 25 and 80 °C.[7] Furthermore, the more flexible polymer matrix facilitated more absorption of water and generate wider ion-conducting channels which leads to high ion conductivity. Generally, the amount of ionic carriers in terms of IEC and the mobility of hydroxide ions are the two main factors governing OH^- conductivity.[1,43] The hydroxide ion conductivity of QPPO/$QSiO_2$-7 reaches the maximum value of 45.08×10^{-2} S cm^{-1} at 80 °C, which is fivefold than the conductivity of QPOSS-based hybrid membranes in our previous work.[22] This might be due to the formation of comparatively more number of reactive sites and hence quaternary ammonium functional groups present in the particles. The intermolecular interaction among the matrix and nano particles generates more ionic clusters as observed in SAXS, which promotes excellent conductivity. After that, high filler concentration creates the membrane structure much more compact and block conducting channels as well as generate more tortuous pathways leading to a visible reduction of OH^- ion transport in the membranes. The relationship between ionic conductivity (σ) and temperature (T) of the QPPO/$QSiO_2$ composite membranes followed Arrhenius behavior, as shown in Figure 7b, and the activation energy (E_a) for ion transport calculated from the slope of the regression line in the plot of ln σ versus 1000/T (°K^{-1}) using the eq 1 is tabulated in Table 2.[7] The pristine QPPO membrane shows an activation energy of 9.15 kJ mol^{-1}. With increasing $QSiO_2$ content, the activation energy increases, indicating that the structures of composites are more compact.[44]

$$\sigma = A \exp(-E_a/RT) \quad (1)$$

where, A is a constant, E_a is the activation energy, R is the universal gas constant (8.314 J K^{-1} mol^{-1}), and T is the absolute temperature (°K). The activation energy of ion conductivity is calculated as E_a = slope × R.

The stability of AEM is a major challenge in alkaline conditions. The long—term alkaline resistance of QPPO/$QSiO_2$ composite membranes was measured by soaking in 1 M KOH solutions at ambient temperature for 1200 h, and the change in conductivity with the time recorded is shown in Figure 7c,d. The conductivity exhibits an increasing trend for the first 100 h in the case of all composite membranes, indicating the absence of polymer backbone scission during that period. The KOH solution might be confined well inside the ionic channels, and OH^- ions could be better solvated in deionized water and participated in ionic conduction, thereby

https://doi.org/10.1021/acsomega.1c00247
ACS Omega 2021, 6, 10168−10179

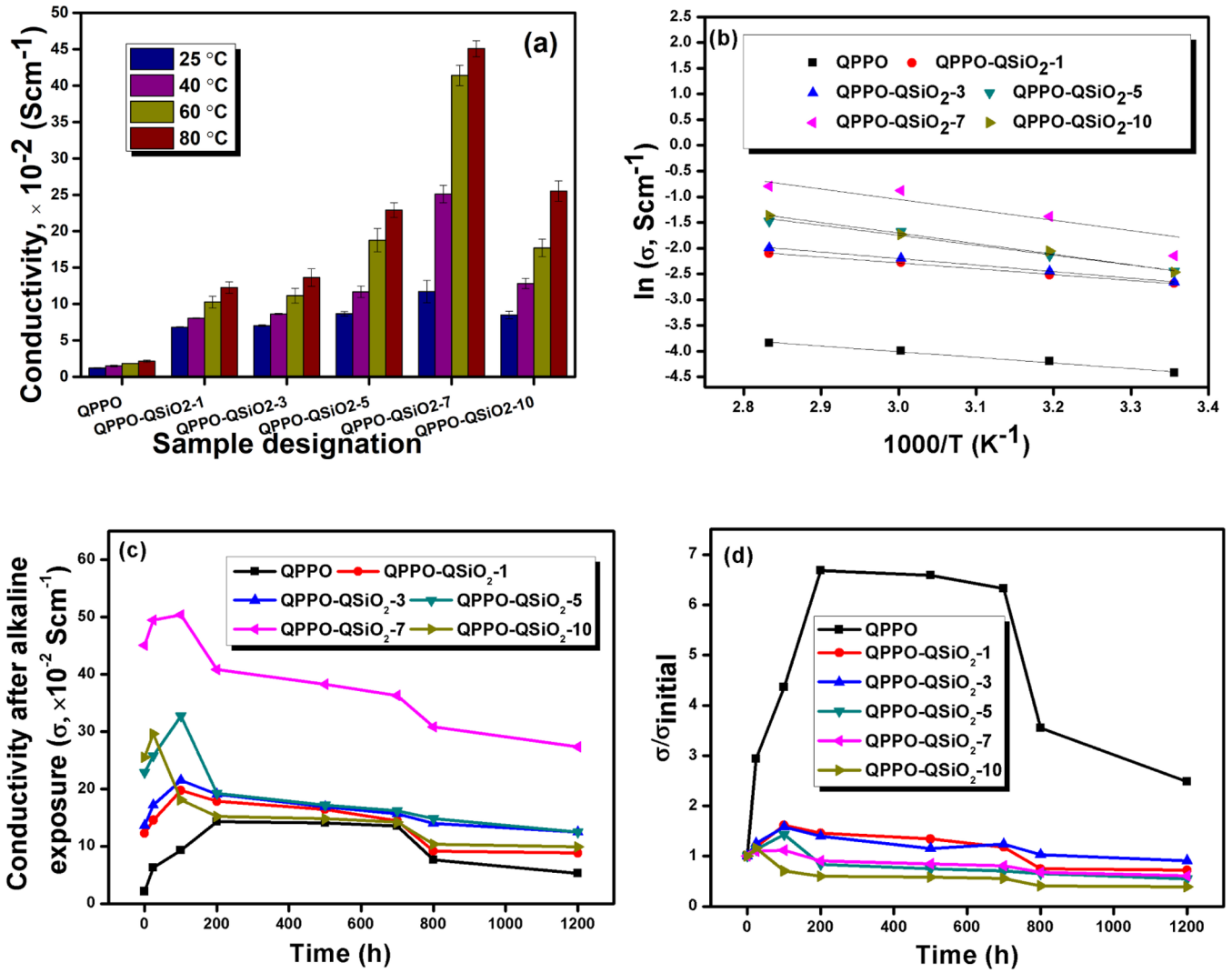

Figure 7. (a) Conductivity, (b) Arrhenius plot for conductivity, (c) change in hydroxide ion conductivity (at 80 °C) with exposure time, and (d) percentage retention of conductivity versus exposure time of QPPO/$QSiO_2$ composite membranes in 1 M KOH solution at ambient temperature.

retarding the quaternary ammonium decomposition.[22] The initial improvement period is higher (200 h) for the pristine QPPO membrane which might be because of the sound participation of KOH solution in conductivity than that in the presence of the nanofiller.[4] After that, conductivity gradually reduces but all the composites maintained about 39−91% of the original conductivity even after 1200 h of alkaline exposure, which demonstrates their good stability. The steric hindrance provided by the trimethylammonium group of QPPO and long glycidyl trimethylammonium alkyl chain in the $QSiO_2$ could be the reason behind the improved chemical stability achieved. The steric hindrance offered by the bulky substituents of $QSiO_2$ protect the organic cations from nucleophilic attack by the excess amount of OH^-. The membrane stability depends on many factors such as the type of alkaline condition, temperature, polymer backbone, and filler structure. The membranes are stable up to seven days of continuous exposure at room temperature in 1 M KOH solution (Table S1). Therefore, we can conclude that the current membranes show reasonably promising alkaline stability in 1 M KOH solution. As the concentration and temperature increase, notably all the membranes are not dissolved in the alkaline solution but experienced a maximum weight loss of about 9.4% after immersion in 5 M KOH solution at 80 °C for 24 h (Tables S1 and S2). The IEC and mechanical properties after alkaline exposure in 1 M KOH for 1200 h at room temperature are given in Table S3. After the alkaline resistance test, QPPO/$QSiO_2$ composite membranes show about 5−22% reduction in their initial IEC, and the results agreed with the change in ionic conductivity after the alkaline stability test. To further verify the alkaline stability of the membranes, Figure S5 shows the comparison of the chemical structure using the FTIR spectra of the tested membranes after alkaline exposure of 1200 h. For all the composite membranes, no obvious change in spectra was observed except for the reduction in the intensity of the peak at around 3500 cm^{-1} corresponding to −NH stretching which could be due to the degradation of the quaternary ammonium group present in the system. No significant change in the characteristic peak position of the aromatic ring and main chain after alkaline treatment indicates that the hydroxide ion only attacks the quaternary ammonium moiety, and the remaining all part of the main chain are unaffected. Composite membranes retain around 92−82% tensile strength and 70−87% elongation after prolonged alkaline exposure, indicating the absence of any significant polymer chain scission and their good mechanical stability in alkaline solution.[32] A similar kind

https://doi.org/10.1021/acsomega.1c00247
ACS Omega 2021, 6, 10168−10179

of degradation is also reported in quaternary ammonium-functionalized polyetherimide membranes. 4.68−5.69% degradation in IEC after exposure in 5 M KOH for 48 h at 30 °C is reported in their study.[45] Degradation of ammonium groups in quaternized polysulfone (QPSU) and QAPOSS is also verified by Elumalai and Sangeetha with 8−10% loss in IEC of QPSU/QAPOSS composites after treatment in 1 M KOH for 7 days at 60 °C.[46]

2.2.6. Single H_2/O_2 Alkaline Fuel Cell Performance. Figure 8 shows the polarization and power density curves of H_2/O_2 single-cell assembled with QPPO/$QSiO_2$-1 and QPPO/$QSiO_2$-3 membranes operated at 60 °C and RH of 100%. Even though the membranes with higher filler loading (above 3 wt %) exhibit higher conductivity than QPPO/$QSiO_2$-3, they cannot be assembled due to the damage of the membrane electrode assembly (MEA). The MEA failure analysis by visual examination displays that tear is the failure mode (Figure S6). The comparatively higher swelling and compression force during single AEM fuel cell fabrication might be the reason behind the MEA failure. Both QPPO/$QSiO_2$-1 and QPPO/$QSiO_2$-3 membranes are mechanically robust and endured compression in the fuel cell without any damage. An open-circuit voltage of 1.01 V is achieved for the QPPO/$QSiO_2$-3 membrane, which is close to the theoretical value (1.23 V) indicating that the voltage loss due to gas cross-over is negligible. A peak power density of 142 mW cm^{-2} is achieved at a current density of 323 mA cm^{-2} and 0.44 V. This value is much higher than the cell using bis-six-membered N-cyclic as well as *N,N′*-didodecyl-hexyl-bis quaternary ammonium-functionalized PPO membranes reported by Chu et al. and Lee et al., respectively, and PPO/silica hybrid membranes reported by Wu et al.[3,29,47] The cell performance is also higher than the commercially available FAA-3-50 Fumatech AEM (OCV: 0.91; maximum power density: 114 mW cm^{-2} at current density: 266 mA cm^{-2} and 0.43 V). The QPPO/$QSiO_2$-1 membrane exhibits an OCV of 0.87 V and a peak power density of 88 mW cm^{-2} at a current density of 179 mA cm^{-2} and 0.50 V. The cell performances of imidazolium-functionalized graphene oxide filled polysulfone (78.7 mW cm^{-2}) and PPO (136 mW cm^{-2}) are also inferior to those of the present membrane assembled cell.[1,31] However, the fuel cell performance of the composite membrane which exhibited impressive hydroxide ion conductivity is inferior to that of the pristine QPPO membrane. This phenomenon might be attributed to the comparatively higher water content in the presence of $QSiO_2$ which might affect the stability and performance of the fuel cell. Even though the water content and swelling are well within the limit of requirement as per most of the literature published, it is still higher in this study when considered for application.[48,49] Hence, proper water management is important for the best performance of AEMFCs. Although the ionic conductivities and stability of QPPO/$QSiO_2$ membranes could meet the basic necessities of AEMs, water management is still inferior to fuel cell performance. More detailed investigations are required to explain the optimum water content and humidity limit during the fuel cell application. Future work will focus on the fundamental understanding of the effect of swelling on catalyst flooding if any and hence the fuel cell performance.

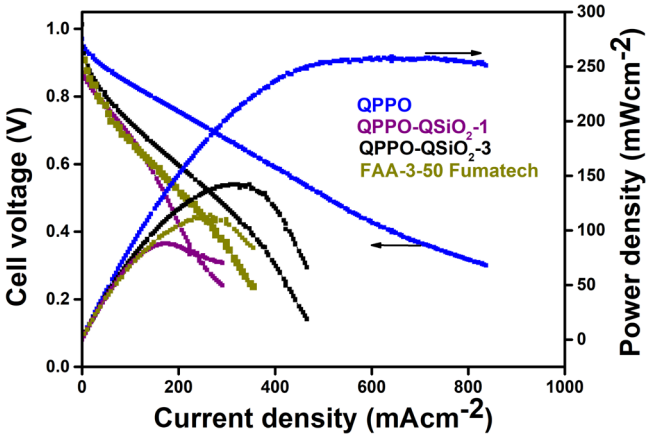

Figure 8. AEMFC performance with the QPPO/$QSiO_2$-3 composite membrane at 60 °C and 100% RH with a H_2/O_2 flow rate of 200/400 cm^3 min^{-1}.

2.2.7. Comparative Study on Present Work and Other Published PPO-Based Membranes. Table 3 summarizes a comparison of the performance properties of the best present composite membrane with different structurally modified PPO and its hybrid membranes reported in the literature. On comparing the published data corresponding to the PPO membranes with piperidinium, N-spirocyclic as well as dodecyl-hexyl quaternary ammonium cations, and polystyrene-grafted quaternized PPO, the QPPO/$QSiO_2$-3 membrane

Table 3. Comparison of Membrane Characteristics between Present Work and Other Published PPO-Based Membranes

sample designation	conductivity ($\times 10^{-2}$ S cm^{-1})	swelling at RT (%)	alkaline stability (% of initial conductivity)	power density (mW cm^{-2})	refs
QPPo/$QSiO_2$-3	13.63 (80 °C) 7.03 (RT)	8.6	91.0 (1 M KOH, 1200 h, RT)	142 (60 °C, RH: 100%)	present work
PPO-ASU-30	7.43 (80 °C)	18.5	98.0 (1 M NaOH, 250 h, 80 °C)	90.2 (60 °C, RH: 100%)	3
PPO-DMP-30	7.05 (80 °C)	18.5	95.0 (1 M NaOH, 250 h, 80 °C)	124.7 (60 °C, RH: 100%)	3
ImPPO/IL-GO-0.5%	7.85 (80 °C)	28.5	70.0 (2 M KOH, 480 h, 80 °C)	136 (60 °C, RH: 100%)	31
PPO-10.8	10.76 (80 °C)		92.1 (1 M KOH, 500 h, 60 °C)	60 (60 °C, RH: 95%)	29
PPO/SiO_2 (5.4%)	2.7(80 °C)			32 (50 °C, RH: 100%)	47
QAPPO-g-PS-31	1.46 (RT)	5.2	80.0 (1 M NaOH, 500 h, 80 °C)	64.4 (60 °C, RH: 100%)	50
m-QPPO-50	4.28 (20 °C)	30.0	85.0 (1 M NaOH, 200 h, 60 °C)	333 (60 °C, RH: 100%)	26
QAPPO/8% IL_1−SiO_2	3.2 (RT) 7.02 (80 °C)	30.0	92.9 (1 M KOH, 720 h, RT)	145.4 (60 °C, RH: 100%)	51
PPO-$CE_{0.10}$-$QA_{0.90}$	11.68 (80 °C)	19.5	95.0 (2 M KOH, 500 h, 80 °C)	350 (80 °C, RH: 100%)	52
BPPO/TEA-1% TiO_2-30 ethyl-IL	5.14 (60 °C)	12.89	72.6 (6 M NaOH, 300 h, RT)		53

https://doi.org/10.1021/acsomega.1c00247
ACS Omega 2021, 6, 10168−10179

Scheme 1. Synthesis of $QSiO_2$

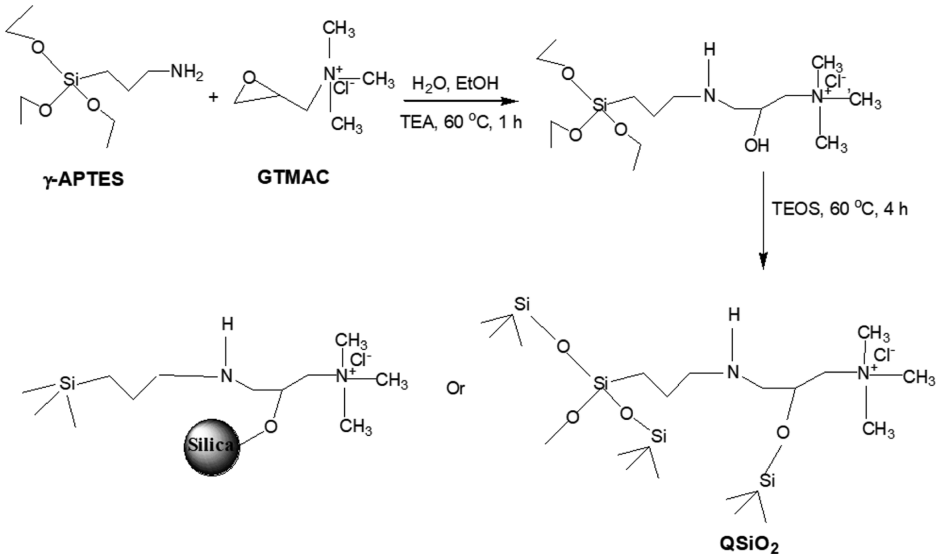

exhibits higher conductivity and fuel cell performances.[3,29,50] The presence of crown-ether crosslinking and isomeric benzyltrimethyl ammonium cations in PPO imparts higher cell performance than the present membrane, but two to three fold higher swelling isobserved.[26] Hybrid PPO membranes based on silica and ionic liquid-grafted graphene oxide as well as titanium dioxide are inferior to QPPO/$QSiO_2$-3 in terms of ionic conductivity and fuel cell performances. The present composite membrane shows the fuel cell performance similar to the QAPPO/8% IL_1−SiO_2 hybrid membrane reported by Chen et al., with comparatively higher chemical and dimensional stability.[51] The long alkyl chain of glycidyltrimethylammonium on silica helps the membrane to reach high stability. Based on the comparatively maximum conductivity and good chemical and dimensional stability obtained for QPPO/$QSiO_2$-3, we expected higher single cell performance than what we attained. Hence, we need more research on the assembly and operating conditions as well as the effect of hydration on the cell performance, and further research is ongoing.

3. SUMMARY AND CONCLUSIONS

In the present work, the ring−opening reaction mediated sol−gel process has been employed in the synthesis of quaternized silica ($QSiO_2$) particles with an average diameter of 5−15 nm. Different proportions of $QSiO_2$ are incorporated into the quaternized poly(2,6-dimethyl-1,4-phenylene oxide) (QPPO) to fabricate a series of novel alkaline anion exchange composite membranes by the simple casting method. The AEMs prepared from QPPO and $QSiO_2$ exhibit a swelling of about 7−11% at RT and 11−22% at 80 °C. The hydroxide ion conductivity is as high as 45.08×10^{-2} S cm^{-1} at 80 °C for QPPO/$QSiO_2$-7 with an IEC of 3.21 meq·g^{-1} and hydration number of 11.15. Moreover, owing to the steric hindrance offered by the long glycidyl trimethyl ammonium alkyl chain grafted in the $QSiO_2$, QPPO/$QSiO_2$-3 AEM demonstrated outstanding alkaline stability, with 91% of retention in hydroxide conductivity after prolonged ageing of 1200 h in 1 M KOH solution at ambient temperature. The composite membrane with 3 wt % $QSiO_2$ content shows the best overall performance and achieved a peak power density of 142 mW cm^{-2} at a current density of 323 mA cm^{-2} and 0.44 V in a single cell. Hence, these membrane shows promise for application in alkaline membrane fuel cells. However, compared to the pristine QPPO membranes, the composite membrane shows performance loss after implementation in the fuel cell. Primary observation after recovery and analysis of AEM from AEMFC suggests that the hydrolytic stability is still inferior to fuel cell performance, and further research is on-going to improve the stability and cell performance.

4. EXPERIMENTAL SECTION

4.1. Materials. Poly(2,6-dimethyl-1,4-phenylene oxide) (PPO, M_w: approximately 50,000 g mol^{-1}) was obtained from Asahi Kasei, Japan. Glycidyltrimethylammonium chloride (GTMAC, >90%), 2,2′-azobis-isobutyronitrile (12 wt % in acetone), trimethylamine, triethylamine (TEA), *N*-bromosuccinimide (99%), γ-APTES, and TEOS were provided by Sigma-Aldrich. Chloro benzene (99%) and *N*-methyl-2-pyrrolidone (NMP, 99%) were received from Samchun Chemicals, Korea. All other chemicals are commercially available and used as received without further purification.

4.2. Synthesis of $QSiO_2$. Quaternized silica was synthesized through the epoxide ring-opening reaction and sol−gel process. 19.2 mL of de-ionized water (1.07 mol), 3.42 mL ethanol (0.059 mol), 1 mL GTMAC (7 mmol), 0.1 mL γ-APTES (0.427 mmol), and 0.081 mL TEA (0.581 mmol) were mixed together at 60 °C for 1 h using an oil bath under a nitrogen atmosphere. The pH value of the solution was about 8. 2.19 mL of TEOS (9.88 mmol) was added into the mixture dropwise within 2 min under continuous stirring for about 4 h at 60 °C under a nitrogen atmosphere. Afterward, the solution was cooled to room temperature, the modified silica ($QSiO_2$) was separated, and the product was washed using de-ionized water and methanol and then dried under vacuum at 60 °C overnight. The schematic representation for $QSiO_2$ synthesis is shown in Scheme 1. The product obtained was in the form of white fluffy powder. Silica without any modification (SiO_2) was also synthesized using the same procedure without using GTMAC.

4.3. Preparation of QPPO/$QSiO_2$ Membranes. QPPO was synthesized using a similar procedure reported in our

https://doi.org/10.1021/acsomega.1c00247
ACS Omega 2021, 6, 10168−10179

previous work, and the degree of quaternization was about 37%, as confirmed by ^{1}H NMR spectroscopy.[22] QPPO/$QSiO_2$ hybrid membranes were fabricated by the solution casting method. A 5% (w/v) QPPO solution was prepared by dissolving 0.25 g of polymer in 5 mL of NMP over a period of 2 h stirring at room temperature. Different quantities of $QSiO_2$ (1, 3, 5, 7, and 10 wt % of QPPO) dispersed in 5 mL of NMP after sonication for 1 h were mixed together with the QPPO solution for 4 h at ambient temperature followed by ultrasonic oscillation for about 30 min. The resultant mixture obtained was then cast onto a clear glass Petri dish and then successfully dried at 60 °C until the solvent was removed (~12 h). Before use, the obtained hybrid composite membranes were soaked in 1 M KOH solution for one day to convert the quaternized membrane into the OH^- form. All the membranes were washed with de-ionized water to remove the unreacted KOH and dried at ambient temperature for 24 h. The final composite membranes' thickness was maintained in the range of 20−30 μm and were designated as QPPO/$QSiO_2$-*X*, where *X* is denoted the weight percentage of $QSiO_2$ to the polymer (*X* = 1, 3, 5, 7 and 10). The control sample without $QSiO_2$ was also prepared by the same method and designated as QPPO.

4.4. Characterization. The FTIR spectra of quaternized silica and membranes were recorded using a Nicolet impact 400, Thermo Scientific spectrometer in the wavenumber range of 4000−600 cm^{-1} at a normal resolution of 4 cm^{-1} with 64 scans. The morphologies of SiO_2 and $QSiO_2$ were characterized by HRTEM (TF30ST-300 kV). The morphology and elemental dot mapping of the composite membranes in the OH^- form were investigated with the help of a field emission scanning electron microscope (FE-SEM, Philips XL 30S FEG) equipped with an EDAX detector. All the samples were subjected to gold sputtering before measurement. SAXS analysis of the dry membranes was carried out with a Rigaku HR-XRD SmartLab diffractometer equipped with a Cu Kα (λ = 1.54 Å) slit collimated X-ray source operating at 45 kV and 200 mA at a scanning rate of 0.25° min^{-1} in a 2θ range from 0 to 2.1°. The measurement was carried out under 50% RH at room temperature.

The mechanical properties were studied by means of a universal testing machine (LR10K, Lloyd Instrument) at RT and a crosshead speed of 10 mm min^{-1}. The TGA was conducted on a TGA Q50, TA Instrument in a temperature range between 30 and 800 °C at a heating rate of 10 °C min^{-1} under a nitrogen atmosphere. The melting temperatures and different transitions of the membranes were determined with the help of DSC (Q 20, TA instrument). The two heating runs, first from 30 to 250 °C and second from 30 to 350 °C, were recorded under a nitrogen atmosphere at a heating and cooling rate of 10 °C min^{-1}.

For water uptake (WU) and swelling measurement, the dried membranes (60 °C, 24 h) were soaked in deionized water for 24 h at ambient temperature (25 °C) and 80 °C. The swelling ratio and WU values were determined from the change of its length and weight, respectively, in swollen and dry states. IEC of the prepared membranes was found at 25 °C using a typical acid−base titration method. The hydration number (λ), number of water molecules absorbed per ion-exchange group, was estimated from

$$\lambda = \frac{\mathrm{WU} \times 1000}{\mathrm{IEC} \times 18} \quad (2)$$

The state of water in the membranes (bound and free/bulk water) was quantified using thermogravimetric analyzer at a heating rate of 10 °C min^{-1} under a nitrogen atmosphere. The bound water was calculated from the percentage weight loss of the hydrated membrane in between 100 and 150 °C and the bulk water obtained from the difference among total WU and bound water content (eq 3).[54] The weight percentage of the membrane at 100 °C was set as 100% and the weight loss at 150 °C was taken as bound water content.

$$\text{Bulk water} = \text{total water content or water uptake (WU)} - \text{bound water content} \quad (3)$$

The detailed procedures for all these characterizations are published in our previous work.[22]

4.4.1. Conductivity and Alkaline Stability. The ionic conductivity was measured by means of electrochemical impedance spectroscopy (SP-300 EIS, Bio Logic Science Instrument) over a frequency range 100 mHz to 1 MHz. Before being mounted on the conductivity cell, the membrane (4 cm × 1 cm) was pretreated in deionized water for 24 h to remove any left-over salt on its surface. The ion conductivity of the membranes was calculated by using the resistance of the membranes according to eq 4

$$\text{conductivity, } \sigma\ (\mathrm{S\ cm^{-1}}) = \frac{L}{R \cdot A} \quad (4)$$

where *R* is the resistance and *A* and *L* are cross-sectional area and thickness of the membranes, respectively.

The chemical stability of the composite membranes in the alkaline environment was determined from the difference of ion conductivities after being submerged in 1 M KOH solution at ambient temperature for 1200 h. The conductivity was determined after different intervals of time at 80 °C in deionized water (σ). Initial ionic conductivity of the membranes ($\sigma_{initial}$) in the OH^- form was recorded. The retention of hydroxide ion conductivity was calculated from the ratio of conductivity after alkaline exposure to the initial conductivity ($\sigma/\sigma_{initial}$). The degradation of the membranes was also studied by measuring weight loss after exposed in different molar concentrations of KOH solutions. The composite membranes dried at 60 °C for 24 h were soaked in various molar concentrations of KOH solutions for definite time duration and weighed after drying at 60 °C for 24 h.

4.4.2. Fuel Cell Performance. The fuel cell performance using the composite membrane was investigated in a single cell at 60 °C and 100% RH. The H_2 and O_2 were supplied at flow rates of 200 and 400 cm^3 min^{-1} to the anode and cathode, respectively. A well-dispersed catalyst ink was prepared by ultra-sonicating a mixture of Pt/C catalysts (Tanaka, 46.2 wt %), 1-propanol, deionized water, and ionomer solution (Fumatech, Fumion FAA—3, 10 wt % in NMP). The as-prepared ink was spray-coated on the membrane (0.4 mg Pt/cm^2) through an air spray gun that resulted in catalyst-coated membranes (CCMs). The assembly of CCMs, gas diffusion layers (Sigracet 39 BCE), and gaskets (Teflon) were used to obtain MEA, and the active electrode area was 5 cm^2.

■ ASSOCIATED CONTENT

Supporting Information

The Supporting Information is available free of charge at https://pubs.acs.org/doi/10.1021/acsomega.1c00247.

https://doi.org/10.1021/acsomega.1c00247
ACS Omega 2021, 6, 10168−10179

Figures including morphology, water content, FTIR spectra of membranes after alkaline treatment, and MEA after fuel cell operation and tables with weight loss, mechanical as well as IEC change after alkaline stability test (PDF)

AUTHOR INFORMATION

Corresponding Author

Sang Yong Nam − *Department of Materials Engineering and Convergence Technology, Gyeongsang National University, Jinju 52828, Republic of Korea;* orcid.org/0000-0002-6056-2318; Email: walden@gnu.ac.kr

Authors

Vijayalekshmi Vijayakumar − *Department of Materials Engineering and Convergence Technology, Gyeongsang National University, Jinju 52828, Republic of Korea*

Tae Yang Son − *Department of Materials Engineering and Convergence Technology, Gyeongsang National University, Jinju 52828, Republic of Korea*

Kwang Seop Im − *Department of Materials Engineering and Convergence Technology, Gyeongsang National University, Jinju 52828, Republic of Korea*

Ji Eon Chae − *Fuel Cell Research Center, Korea Institute of Science and Technology, Seoul 02792, Republic of Korea*

Hyoung Juhn Kim − *Fuel Cell Research Center, Korea Institute of Science and Technology, Seoul 02792, Republic of Korea*

Tae Hyun Kim − *Organic Material Synthesis Laboratory, Department of Chemistry, Incheon National University, Incheon 22012, Republic of Korea;* orcid.org/0000-0002-1654-3785

Complete contact information is available at: https://pubs.acs.org/10.1021/acsomega.1c00247

Notes

The authors declare no competing financial interest.

ACKNOWLEDGMENTS

The authors acknowledge the financial assistance received from the National Research Foundation of Korea (NRF), ministry of science and ICI (NRF—2015 M1A2A2058028). This research was also supported by basic science research program funded by ministry of education (NRF—2020R1A6A1A03038697).

REFERENCES

(1) Mao, X.; Zhao, J.; He, G.; Zhang, Y.; Jiang, Z.; Li, Z.; Li, Z. Enhancing hydroxide conductivity of anion exchange membrane via incorporating densely imidazolium functionalized graphene oxide. *Solid State Ionics* **2019**, *333*, 83−92.

(2) Elumalai, V.; Sangeetha, D. Synergic effect of ionic liquid grafted titanate nanotubes on the performance of anion exchange membrane fuel cell. *J. Power Sources* **2019**, *412*, 586−596.

(3) Chu, X.; Liu, L.; Huang, Y.; Guiver, M. D.; Li, N. Practical implementation of bis-six-membered N-cyclic quaternary ammonium cations in advanced anion exchange membranes for fuel cells: Synthesis and durability. *J. Membr. Sci.* **2019**, *578*, 239−250.

(4) Wang, E. D.; Zhao, T. S.; Yang, W. W. Poly (vinyl alcohol)/3-(trimethylammonium) propyl-functionalized silica hybrid membranes for alkaline direct ethanol fuel cells. *Int. J. Hydrogen Energy* **2010**, *35*, 2183−2189.

(5) Elumalai, V.; Sangeetha, D. Preparation of anion exchangeable titanate nanotubes and their effect on anion exchange membrane fuel cell. *Mater. Des.* **2018**, *154*, 63−72.

(6) Huang, C.-Y.; Lin, J.-S.; Pan, W.-H.; Shih, C.-M.; Liu, Y.-L.; Lue, S. J. Alkaline direct ethanol fuel cell performance using alkali-impregnated polyvinyl alcohol/functionalized carbon nano-tube solid electrolytes. *J. Power Sources* **2016**, *303*, 267−277.

(7) Feng, T.; Lin, B.; Zhang, S.; Yuan, N.; Chu, F.; Hickner, M. A.; Wang, C.; Zhu, L.; Ding, J. Imidazolium-based organic-inorganic hybrid anion exchange membranes for fuel cell applications. *J. Membr. Sci.* **2016**, *508*, 7−14.

(8) Pan, J.; Zhu, L.; Han, J.; Hickner, M. A. Mechanically tough and chemically stable anion exchange membranes from rigid-flexible semi-interpenetrating networks. *Chem. Mater.* **2015**, *27*, 6689−6698.

(9) Guo, D.; Zhuo, Y. Z.; Lai, A. N.; Zhang, Q. G.; Zhu, A. M.; Liu, Q. L. Interpenetrating anion exchange membranes using poly(1-vinylimidazole) as bifunctional crosslinker for fuel cells. *J. Membr. Sci.* **2016**, *518*, 295−304.

(10) Xiong, Y.; Liu, Q. L.; Zhu, A. M.; Huang, S. M.; Zeng, Q. H. Performance of organic-inorganic hybrid anion-exchange membranes for alkaline direct methanol fuel cells. *J. Power Sources* **2009**, *186*, 328−333.

(11) Barkoula, N.-M.; Alcock, B.; Cabrera, N. O.; Peijs, T. Fatigue properties of highly oriented polypropylene tapes and all-polypropylene composites. *Polym. Polym. Compos.* **2008**, *16*, 101−113.

(12) Wang, Y.; Wan, H.; Wang, J.; Wang, L.; Feng, R. Hydroxide ion highway constructed by orderly aligned quaternary ammonium groups in anion exchange membranes. *J. Electrochem. Soc.* **2017**, *164*, F1051−F1062.

(13) Xiao Lin, C.; Qin Wang, X.; Ning Hu, E.; Yang, Q.; Gen Zhang, Q.; Mei Zhu, A.; Lin Liu, Q. Quaternized triblock polymer anion exchange membranes with enhanced alkaline stability. *J. Membr. Sci.* **2017**, *541*, 358−366.

(14) Abuin, G. C.; Franceschini, E. A.; Nonjola, P.; Mathe, M. K.; Modibedi, M.; Corti, H. R. A high selectivity quaternized polysulfone membrane for alkaline direct methanol fuel cells. *J. Power Sources* **2015**, *279*, 450−459.

(15) Gong, Y.; Liao, X.; Xu, J.; Chen, D.; Zhang, H. Novel anion-conducting interpenetrating polymer network of quaternized polysulfone and poly(vinyl alcohol) for alkaline fuel cells. *Int. J. Hydrogen Energy* **2016**, *41*, 5816−5823.

(16) Li, Z.; Zhang, Y.; Cao, T.; Yang, Y.; Xiong, Y.; Xu, S.; Xu, Z. Highly conductive alkaline anion exchange membrane containing imidazolium-functionalized octaphenyl polyhedral oligomeric silsesquioxane filler. *J. Membr. Sci.* **2017**, *541*, 474−482.

(17) Miao, L.; Wang, X.; Fu, Y.; Hu, B.; Bai, Y.; Lü, C. Quaternized polyhedral oligomeric silsesquioxanes (qposs) modified polysulfone-based composite anion exchange membranes. *Solid State Ionics* **2017**, *309*, 170−179.

(18) Vijayakumar, E.; Sangeetha, D. A Quaternized mesoporous silica/polysulfone composite membrane for an efficient alkaline fuel cell application. *RSC Adv.* **2015**, *5*, 42828−42835.

(19) Liu, L.; Hu, B.; He, Y.; Zhao, Y.; Tong, C.; Lu, C. Novel quaternized mesoporous silica nanoparticle modified polysulfone-based composite anion exchange membranes for alkaline fuel cells. *RSC Adv.* **2015**, *5*, 43381−43390.

(20) Tripathi, B. P.; Kumar, M.; Shahi, V. K. Organic-inorganic hybrid alkaline membranes by epoxide ring opening for direct methanol fuel cell applications. *J. Membr. Sci.* **2010**, *360*, 90−101.

(21) He, S. S.; Strickler, A. L.; Frank, C. W. A semi-interpenetrating network approach for dimensionally stabilizing highly-charged anion exchange membranes for alkaline fuel cells. *ChemSusChem* **2015**, *8*, 1472−1483.

(22) Vijayakumar, V.; Son, T. Y.; Kim, H. J.; Nam, S. Y. A facile approach to fabricate poly(2,6-dimethyl-1,4-phenylene oxide) based anion exchange membranes with extended alkaline stability and ion conductivity for fuel cell applications. *J. Membr. Sci.* **2019**, *591*, 117314.

(23) Wu, Y.; Wu, C.; Xu, T.; Yu, F.; Fu, Y. Novel anion-exchange organic-inorganic hybrid membranes: Preparation and characterizations for potential use in fuel cells. *J. Membr. Sci.* **2008**, *321*, 299−308.
(24) Charradi, K.; Ahmed, Z.; Aranda, P.; Chtourou, R. Silica/montmorillonite nanoarchitectures and layered double hydroxide-SPEEK based composite membranes for fuel cells applications. *Appl. Clay Sci.* **2019**, *174*, 77−85.
(25) Elumalai, V.; Dharmalingam, S. Synthesis characterization and performance evaluation of ionic liquid immobilized SBA-15 /quaternised polysulfone composite membrane for alkaline fuel cell. *Microporous Mesoporous Mater.* **2016**, *236*, 260−268.
(26) Liu, L.; Liu, Z.; Bai, L.; Shao, C.; Chen, R.; Zhao, P.; Chu, X.; Li, N. Quaternized Poly (2, 6-dimethyl-1, 4-phenylene oxide) anion exchange membranes based on isomeric benzyltrimethylammonium cations for alkaline fuel cells. *J. Membr. Sci.* **2020**, *606*, 118133.
(27) Becerra-Arciniegas, R.-A.; Narducci, R.; Ercolani, G.; Antonaroli, S.; Sgreccia, E.; Pasquini, L.; Knauth, P.; Di Vona, M. L. Alkaline stability of model anion exchange membranes based on poly(phenylene oxide) (ppo) with grafted quaternary ammonium groups: Influence of the functionalization route. *Polymer* **2019**, *185*, 121931.
(28) Gong, X.; He, G.; Wu, Y.; Zhang, S.; Chen, B.; Dai, Y.; Wu, X. Aligned electrospun nanofibers as proton conductive channels through thickness of sulfonated poly (phthalazinone ether sulfone ketone) proton exchange membranes. *J. Power Sources* **2017**, *358*, 134−141.
(29) Lee, B.; Lim, H.; Chae, J. E.; Kim, H.-J.; Kim, T.-H. Physically-Crosslinked anion exchange membranes by blending ionic additive into alkyl-substituted quaternized PPO. *J. Membr. Sci.* **2019**, *574*, 33−43.
(30) Martinez, N.; Gebel, G.; Blanc, N.; Boudet, N.; Micha, J.-S.; Lyonnard, S.; Morin, A. Heterogeneous nanostructural aging of fuel cell ionomer revealed by operando SAXS. *ACS Appl. Energy Mater.* **2019**, *2*, 3071−3080.
(31) Yang, Q.; Lin, C. X.; Liu, F. H.; Li, L.; Zhang, Q. G.; Zhu, A. M.; Liu, Q. L. Poly (2,6-dimethyl-1,4-phenylene oxide)/ionic liquid functionalized graphene oxide anion exchange membranes for fuel cells. *J. Membr. Sci.* **2018**, *552*, 367−376.
(32) Zhang, X.; Chu, X.; Zhang, M.; Zhu, M.; Huang, Y.; Wang, Y.; Liu, L.; Li, N. Molecularly designed, solvent processable tetraalkylammonium-functionalized fluoropolyolefin for durable anion exchange membrane fuel cells. *J. Membr. Sci.* **2019**, *574*, 212−221.
(33) Ge, Q.; Liang, X.; Ding, L.; Hou, J.; Miao, J.; Wu, B.; Yang, Z.; Xu, T. Guiding the self-assembly of hyperbranched anion exchange membranes utilized in alkaline fuel cells. *J. Membr. Sci.* **2019**, *573*, 595−601.
(34) Vijayakumar, V.; Khastgir, D. Hybrid composite membranes of chitosan/sulfonated polyaniline/silica as polymer electrolyte membrane for fuel cells. *Carbohydr. Polym.* **2018**, *179*, 152−163.
(35) Wang, K.; Gao, L.; Liu, J.; Su, X.; Yan, X.; Dai, Y.; Jiang, X.; Wu, X.; He, G. Comb-shaped ether-free poly(biphenyl indole) based alkaline membrane. *J. Membr. Sci.* **2019**, *588*, 117216.
(36) Al Munsur, A. Z.; Hossain, I.; Nam, S. Y.; Chae, J. E.; Kim, T.-H. Quaternary ammonium-functionalized hexyl bis(quaternary ammonium)-mediated partially crosslinked SEBSs as highly conductive and stable anion exchange membranes. *Int. J. Hydrogen Energy* **2020**, *45*, 15658−15671.
(37) Wang, B.; Zhu, Y.; Zhou, T.; Xie, K. Synthesis and properties of chitosan membranes modified by reactive cationic dyes as a novel alkaline exchange membrane for low temperature fuel cells. *Int. J. Hydrogen Energy* **2016**, *41*, 18166−18177.
(38) Liu, W.; Liang, N.; Peng, P.; Qu, R.; Chen, D.; Zhang, H. Anion-exchange membranes derived from quaternized polysulfone and exfoliated layered double hydroxide for fuel cells. *J. Solid State Chem.* **2017**, *246*, 324−328.
(39) Zheng, X.; Song, S. Y.; Yang, J. R.; Wang, J. L.; Wang, L. 4-Formyl dibenzo-18-crown-6 grafted polyvinyl alcohol as anion exchange membranes for fuel cell. *Eur. Polym. J.* **2019**, *112*, 581−590.
(40) Liu, J.; Yan, X.; Gao, L.; Hu, L.; Wu, X.; Dai, Y.; Ruan, X.; He, G. Long-branched and densely functionalized anion exchange membranes for fuel cells. *J. Membr. Sci.* **2019**, *581*, 82−92.
(41) Bae, I.; Oh, K.-H.; Yun, S.-H.; Kim, H. Asymmetric silica composite polymer electrolyte membrane for water management of fuel cells. *J. Membr. Sci.* **2017**, *542*, 52−59.
(42) Singh, S.; Jasti, A.; Kumar, M.; Shahi, V. K. A Green method for the preparation of highly stable organic-inorganic hybrid anion-exchange membranes in aqueous media for electrochemical processes. *Polym. Chem.* **2010**, *1*, 1302−1312.
(43) Lin, B.; Xu, F.; Su, Y.; Han, J.; Zhu, Z.; Chu, F.; Ren, Y.; Zhu, L.; Ding, J. Ether-free polybenzimidazole bearing pendant imidazolium groups for alkaline anion exchange membrane fuel cells application. *ACS Appl. Energy Mater.* **2020**, *3*, 1089−1098.
(44) Wang, L.-L.; Wang, J.-L.; Zhang, Y.; Feng, R.-j. Alkaline hybrid composite membrane for direct methanol fuel cells application. *J. Electroanal. Chem.* **2015**, *759*, 174−183.
(45) Yadav, V.; Rajput, A.; Sharma, P. P.; Jha, P. K.; Kulshrestha, V. Polyetherimide based anion exchange membranes for alkaline fuel cell: Better ion transport properties and stability. *Colloids Surf., A* **2020**, *588*, 124348.
(46) Elumalai, V.; Sangeetha, D. Anion Exchange composite membrane based on octa quaternary ammonium polyhedral oligomeric silsesquioxane for alkaline fuel cells. *J. Power Sources* **2018**, *375*, 412−420.
(47) Wu, Y.; Wu, C.; Varcoe, J. R.; Poynton, S. D.; Xu, T.; Fu, Y. Novel silica/poly(2,6-dimethyl-1,4-phenylene oxide) hybrid anion-exchange membranes for alkaline fuel cells: effect of silica content and the single cell performance. *J. Power Sources* **2010**, *195*, 3069−3076.
(48) Lin, B.; Xu, F.; Chu, F.; Ren, Y.; Ding, J.; Yan, F. bis-imidazolium based poly(phenylene oxide) anion exchange membranes for fuel cells: The effect of cross-linking. *J. Mater. Chem. A* **2019**, *7*, 13275−13283.
(49) Zhu, Y.; Ding, L.; Liang, X.; Shehzad, M. A.; Wang, L.; Ge, X.; He, Y.; Wu, L.; Varcoe, J. R.; Xu, T. Beneficial use of rotatable-spacer side-chains in alkaline anion exchange membranes for fuel cells. *Energy Environ. Sci.* **2018**, *11*, 3472−3479.
(50) Yang, C.; Liu, L.; Huang, Y.; Dong, J.; Li, N. Anion-conductive poly(2,6-dimethyl-1,4-phenylene oxide) grafted with tailored polystyrene chains for alkaline fuel cells. *J. Membr. Sci.* **2019**, *573*, 247−256.
(51) Chen, N.; Liu, Y.; Long, C.; Li, R.; Wang, F.; Zhu, H. Enhanced performance of ionic-liquid-coated silica/quaternized poly(2,6-dimethyl-1,4-phenylene oxide) composite membrane for anion exchange membrane fuel cells. *Electrochim. Acta* **2017**, *258*, 124−133.
(52) Yang, Q.; Li, L.; Gao, X. L.; Wu, H. Y.; Liu, F. H.; Zhang, Q. G.; Zhu, A. M.; Zhao, C. H.; Liu, Q. L. Crown ether bridged anion exchange membranes with robust alkaline durability. *J. Membr. Sci.* **2019**, *578*, 230−238.
(53) Chen, Y.; Li, Z.; Chen, N.; Li, R.; Zhang, Y.; Li, K.; Wang, F.; Zhu, H. A new method for improving the conductivity of alkaline membrane by incorporating TiO2- ionic liquid composite particles. *Electrochim. Acta* **2017**, *255*, 335−346.
(54) Vijayalekshmi, V.; Khastgir, D. Chitosan/partially sulfonated poly(vinylidene fluoride) blends as polymer electrolyte membranes for direct methanol fuel cell applications. *Cellulose* **2018**, *25*, 661−681.

https://doi.org/10.1021/acsomega.1c00247
ACS Omega 2021, 6, 10168−10179